WIND ENERGY
Wind Energ. 2011; **14**:449–462
Published online 26 November 2010 in Wiley Online Library (wileyonlinelibrary.com). DOI: 10.1002/we.435

RESEARCH ARTICLE

Investigation of the load reduction potential of two trailing edge flap controls using CFD

Joachim Heinz, Niels N. Sørensen and Frederik Zahle

Risø DTU National Laboratory for Sustainable Energy, Wind Energy Department, Roskilde, Denmark

ABSTRACT

In this work, a 2D aero-servo-elastic model of an airfoil section with 3 degrees of freedom (DOF) based on the 2D CFD solver EllipSys2D to calculate the aerodynamic forces is utilized to calculate the load reduction potential of an airfoil equipped with an adaptive trailing edge flap (ATEF) and subjected to a turbulent inflow signal.

The employed airfoil model corresponds to a successfully tested prototype airfoil where piezoelectric actuators were used for the flapping. In the present investigation two possible control methods for the flap are compared in their ability to reduce the fluctuating normal forces on the airfoil due to a 4 s turbulent inflow signal and the best location of the measurement point for the respective control input is determined. While Control 1 uses the measurements of a Pitot tube mounted in front of the leading edge (LE) as input, Control 2 uses the pressure difference between the pressure and suction side of the airfoil measured at a certain chord position.

Control 1 achieves its maximum load reduction of $R_{Std(F_y)} = 76.7\%$ for the shortest Pitot tube of the test, i.e. a Pitot tube with a length of 0.05% of the chord length. Control 2 shows the highest load reduction of $R_{Std(F_y)} = 77.7\%$ when the pressure difference is measured at a chord position of approximately 15%.

KEYWORDS

trailing edge flaps; load alleviation; fatigue loads; control; CFD; wind turbine

Correspondence

J. Heinz, Risø DTU National Laboratory for Sustainable Energy, Wind Energy Division, Building VEA-118, P.O. Box 49, Frederiksborgvej 399, DK 4000, Roskilde, Denmark.
E-mail: jhei@risoe.dtu.dk

Received 14 November 2009; Revised 25 May 2010; Accepted 23 September 2010

1. INTRODUCTION

During normal operation, wind turbine blades are constantly subjected to fluctuating inflow conditions. This is due to the unsteady nature of the wind, the influence of the tower, wind shear effects and operation in yawed conditions. The fluctuations in the inflow cause constantly changing loads on the blades, which can, in turn, cause fatigue damage. Reducing the fatigue loads on the blades can lead to lighter blades and reduce the loads on other components such as bearings, drive train and tower. As a consequence, the lifetime and the size of the wind turbines can be increased, making wind energy potentially cheaper and even more competitive to other energy sources.

Investigations of using a pitching mechanism to alleviate these fatigue loads have shown promising results,[1] but recent studies have shown that even higher load reductions may be possible by using more sophisticated load control techniques with a deformable trailing edge geometry (DTEG).[2–4] The two large advantages of DTEG's compared to a pitching mechanism is that the devices can be actuated individually along the radius of the blade and that smaller masses have to be moved.

Previous work at Risø DTU showed a high potential of load alleviation using adaptive trailing edge flaps (ATEF).[5–9] With a 2D aero-servo-elastic model, using the potential flow solver developed by Gaunaa[10] for the aerodynamic modelling, Buhl *et al.*[5] showed that the standard deviation of the normal force on a 2D airfoil section suspended with springs

and dampers could be reduced with up to 81% if the airfoil is subjected to a turbulent wind field with 10% turbulence intensity. A comparable 2D study by Heinz,[8] calculating the aerodynamic forces with the incompressible Reynolds averaged CFD solver EllipSys2D, led to a reduction in flapwise blade motion of up to 82% while exposing the airfoil to a turbulent inflow.

In the present work, the 2D aero-servo-elastic model of Heinz will be used for a comprehensive parameter study in order to find the preferable sensor positions for two different flap controls. While Control 1 senses the local angle of attack measured with a Pitot tube in front of the leading edge, Control 2 uses the pressure difference between the suction and pressure side at a certain chord position as control input.

2. INVESTIGATED AIRFOIL

The investigations focus on a Risø B1-18 airfoil equipped with THUNDER TH-6R piezoelectric actuators [see Figure 1 (left)] corresponding to a prototype already built at Risø DTU and successfully tested in the VELUX wind tunnel.[6] Thus, the results of the aero-servo-elastic simulations will give information about the load reduction potential of an already existing and available flapping mechanism which is intented to be tested on a Vestas V27 turbine at the end of 2009. Piezoelectric elements are considered in the actual design of ATEF because they ensure a smooth transition between airfoil and flap, and thus reduce the risk of flow separation and noise development.

An accurate measuring of the overall airfoil geometry is rather difficult to accomplish; hence, the coordinates of the prototype surface are found by combining the well-known geometries of the two single components, the Risø B1-18 and the THUNDER TH-6R actuator. The deformation shape of the actuator can be defined via its footprint size and dome height which are given in the manufacturer's data sheet in dependency of the applied voltage. In Figure 1 (right) the resulting airfoil deflections for the maximal applicable voltages of –750 V and –450 V are shown. It is common to describe the flap deflection by a flap angle β where the line through flap hinge point and flap tip is used as reference. For an applied voltage of 0 V the flap angle is defined with $\beta = 0°$. Moving the flap upwards (applying a positive voltage) leads to a negative β, moving the flap downwards (applying a negative voltage) leads to a positive β.

3. METHOD

To investigate the load reduction potential of the prototype airfoil with attached TE flaps, a 2D aero-servo-elastic system is set up. Information about the implemented structural and aerodynamic model, as well as information about the used control strategies, is given below.

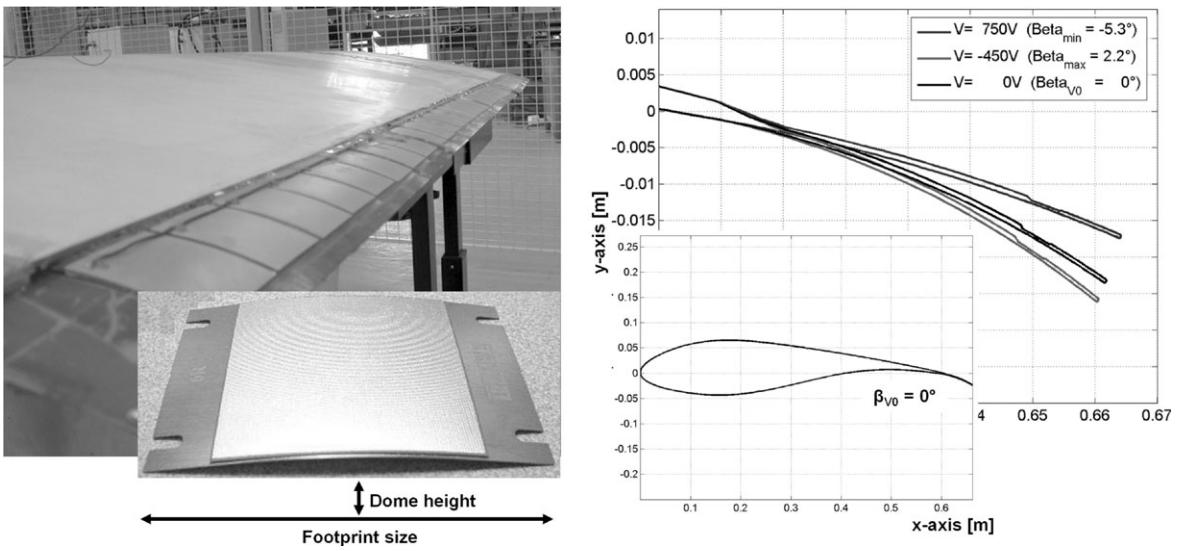

Figure 1. (left) Prototype Airfoil and the THUNDER-TH-R6 Actuator; (right) Generated Airfoil Surface and the Maximum Flap Deflections.

Wind Energ. 2011; **14**:449–462 © 2010 John Wiley & Sons, Ltd.
DOI: 10.1002/we

3.1. Structural model

Figure 2 (left) shows the implemented structural model consisting of a 2D airfoil section, which is assumed to be situated at a certain radial position of a turbine blade. The rigid airfoil section is suspended with linear springs and dampers in order to allow structural motion in the directions of x_{struct}, y_{struct} and θ_{struct}, and thus mimicking the blade dynamics at the given radial section. The springs and dampers are attached at the rotational center RC of the airfoil. The x-axis of the structural coordinate system is aligned with the rotorplane, the y-axis is perpendicular to the rotorplane. The aerodynamic forces F_x and F_y out of the aerodynamic model have to be known in the same directions.

The airfoil is modeled as a rigid body with a point mass m situated at the center of gravity CG. CG is located at a distance l from the rotational center RC. θ_{geom} is the pitch angle of the blade and basically acts like an offset angle which moves the equilibrium state ($\theta_{struct} = 0$) from the rotorplane to the chordline of the airfoil. The equations of motion for this 3 DOF model are given as

$$\begin{aligned} m\ddot{x}_{struct} + c_x\dot{x}_{struct} + k_x x_{struct} &= F_x + ml\dot{\theta}^2_{struct}\cos(\theta_{struct} + \theta_{geom}) \\ &\quad + ml\ddot{\theta}_{struct}\sin(\theta_{struct} + \theta_{geom}) \\ m\ddot{y}_{struct} + c_y\dot{y}_{struct} + k_y y_{struct} &= F_y + ml\dot{\theta}^2_{struct}\sin(\theta_{struct} + \theta_{geom}) \\ &\quad - ml\ddot{\theta}_{struct}\cos(\theta_{struct} + \theta_{geom}) \\ (I_{CG} + ml^2)\ddot{\theta}_{struct} + c_\theta\dot{\theta}_{struct} + k_\theta\theta_{struct} &= F_\theta + ml\ddot{x}_{struct}\sin(\theta_{struct} + \theta_{geom}) \\ &\quad - ml\ddot{y}_{struct}\cos(\theta_{struct} + \theta_{geom}) \end{aligned}$$

where I_{CG} is the moment of inertia around CG. The structural model is a pure 2D model with no additional terms accounting for the blade rotation.

The structural model used in this work is the same as in the works of Buhl *et al.*[5] and Andersen,[7] and the several structural quantities, like spring stiffnesses, damping coefficients and mass of the airfoil section are defined identically (see Table I). The only deviation is that the signs of the angles θ_{geom} and θ_{struct}, as well as the sign of the moment F_θ, have been altered in order to conform with the sign conventions of EllipSys2D.

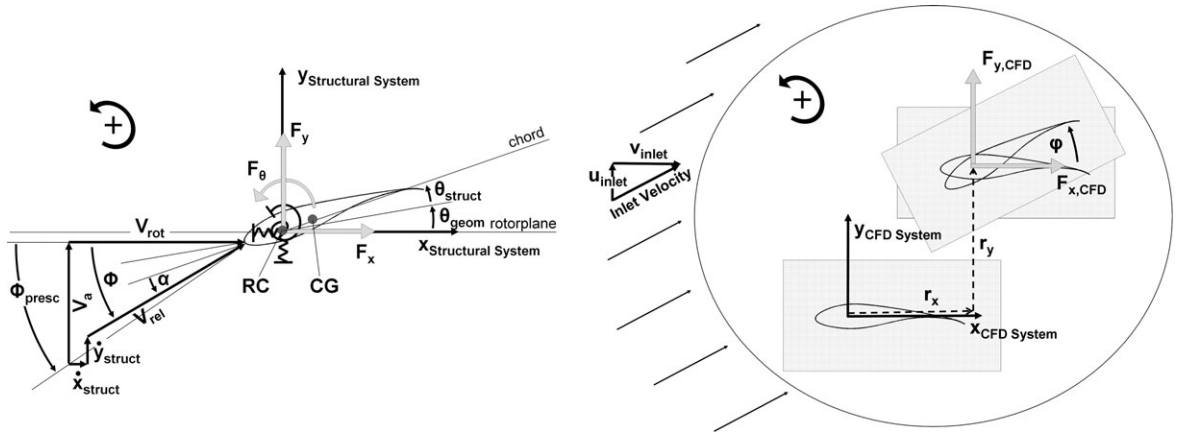

Figure 2. (left) Structural Model; (right) Movable Mesh in EllipSys2D.

Table I. Structural quantities used in this work.

Chord length	1 m	k_x	6316 N/m
RC (distance from LE)	0.30 m	k_y	1579 N/m
CG (distance from LE)	0.35 m	k_θ	8290 N/rad
m (per unit depth)	40 kg	c_x, c_y, c_θ	0 Ns/m
θ_{geom}	5 °		

3.2. Aerodynamic model (EllipSys2D)

The aero-servo-elastic modelling is using the 2D CFD code EllipSys2D to determine the aerodynamic forces on the profile. This code was developed by Michelsen[11,12] and Sørensen,[13] and solves the incompressible Reynolds averaged Navier-Stokes equations (RANS) using primitive variables (u, v and p) in curvilinear coordinates through a multiblock finite volume discretization approach. For incompressible flow, an additional equation is needed for the pressure, and the standard practice is to derive a pressure equation (Poisson equation) by combining the continuity equation with the momentum equations. The momentum and pressure equations are then used in a predictor-corrector fashion (PISO algorithm) to determine the pressure and velocities of the new time step. The third order accurate QUICK scheme is used to project the convective velocities to the cell faces. Information about the PISO algorithm and the QUICK scheme can be found in Ferziger and Peric.[14] The overall EllipSys2D computations are proven to be second-order accurate both in time and in space.

The $k-\omega$ *SST* (Shear Stress Transport) turbulence model by Menter[15] was used in this work. The model has been proven to give very promissing results for 2D airfoil flows.[16] All simulations in this work are carried out under the assumption of a fully turbulent flow.

The grid generation is accomplished with HypGrid2D developed by Sørensen.[17] The grid generator is using a hyperbolic mesh generation procedure, based on an equation of orthogonality and an equation for the cell face area. The generated grid can be seperated in several blocks of prescribed size in order to allow parallel (multiblock) computations. The grid used in this work is of the O-mesh type and consists of 256 cells into the tangential direction ξ and 128 cells into the normal direction η. The domain height was set to $h_{Tot} = 20 \cdot c$ and the height of the first cell adjacent to the surface was set to $h_{\eta=1,2} = 10^{-6} \cdot c$ corresponding to a maximum y^+ value of approximately 0.2. A grid study carried out in Heinz[8] showed that this grid, together with a non-dimensional time step size of $\Delta t^* = 0.01$, is suitable for a reduced pitching frequency of at least $k = 0.084$ and a reduced flapping frequency of at least $k = 0.518$. These frequencies will not be exceeded in the present load reduction investigations. The domain height of $h_{Tot} = 20 \cdot c$ is considered to be sufficient since a comparable computation with a domain height of $h_{Tot} = 140 \cdot c$ and using the turbulent inflow signal of the present work resulted in a maximum deviation in lift of only $\Delta C_l = 3 \cdot 10^{-4}$. The time step size for all presented calculations is set to $\Delta t^* = 0.01$.

Moving the grid / Inlet velocity

In order to simulate the structural motion of the airfoil EllipSys2D provides a routine that moves the grid. This routine accounts for the additional fluxes that arise when the cell vertices are moved. As indicated in Figure 2 (right), the translatoric motions r_x and r_y as well as a rotation φ are feasible.

Besides changing the rotational angle φ of the moving mesh, the angle between airfoil and inflow can also be adjusted with the two inlet velocity components u_{inlet} and v_{inlet} at the domain boundaries.

Morphing the grid

The flap motion of the airfoil is accomplished by using the two extreme flap deflections with $\beta = 2.2°$ and $\beta = -5.3°$ shown in Figure 1 (right). The actual grid is then generated by a linear interpolation between the grid points of these two meshes. The morphing is a subset of the moving mesh algorithm and the additional fluxes due to the changing cell vertices are determined collectively at the end of the moving mesh routine.

By using linear interpolation, the respective grid points move on a straight line from the maximum to the minimum flap configuration. This does not exactly correspond to the real flap motion, where the points move on an arc around the flap hinge point. However, for small changes in the flap angle β, the introduced error is negligible.

Simulating the structural motion

In Figure 2 (left), the structural motions of the considered airfoil section, as well as the corresponding flowfield in front of the airfoil, are shown. The structural motion in x_{struct} and y_{struct} and their influences to the flowfield via $\dot{x}_{struct}$ and $\dot{y}_{struct}$ are simulated by a certain translatoric motion of the grid using the variables r_x and r_y in EllipSys2D. The structural deflection around the rotational centre θ_{struct} as well as the pitch angle of the blade θ_{geom} are simulated by rotating the grid using the variable φ.

Simulating the fluctuating inflow

As illustrated in Figure 2 (left), the flowfield, and thus the resulting AOA in front of the investigated airfoil section, is not only influenced by the three structural motions x_{struct}, y_{struct} and θ_{struct} and the offset angle θ_{geom}. In order to entirely describe the flow in front of the airfoil the rotational velocity V_{rot} and the axial velocity vector V_a, together forming the

Wind Energ. 2011; **14**:449–462 © 2010 John Wiley & Sons, Ltd.
DOI: 10.1002/we

prescribed flowangle ϕ_{presc},* have to be given. The simulations in the present work are carried out with a constant rotational velocity of $V_{rot} = 60$ m s^{-1}. A fluctuating inflow is then described by changing the axial velocity V_a over time, representing the incoming wind which is assumed to be perpendicular to the rotor plane.

There are two different methods conceivable of how the provided input parameters of EllipSys2D [see Figure 2 (right)] can be used to adjust the time-dependent flow angle and to thus simulate a fluctuating inflow.

- Method 1: Using the inlet velocity components u_{inlet} and v_{inlet} to describe the velocity components V_a and V_{rot}.
- Method 2: Keeping the inlet velocity components with $u_{inlet} = 0$ and $v_{inlet} = 1$ constant† and instead rotating the whole airfoil with $\varphi = -\phi_{presc}$.
  It is important to notice that this additional rotation with $-\phi_{presc}$ is only accomplished in the aerodynamic part of the model in order to adjust the correct AOA and to calculate the correct aerodynamic forces. The structural model is not affected by this rotation and no additional inertia terms or any other additional loadings on the three DOF's will arise, since the only information assigned from the aerodynamic model to the structural model is the resulting aerodynamic forces $F_{x,CFD}$, $F_{y,CFD}$ and $F_{\theta,CFD}$ — transformed into the directions of the structural coordinate system.

Method 1, illustrated in Figure 3 (left), is quite intuitive and seems to be straightforward, but the implementation of the method is linked to several problems. EllipSys2D is an incompressible flow solver, and the mass fluxes into and out of the computational domain have thus to be equal at each time step. If the inlet velocity components u_{inlet} and v_{inlet} are used to describe the fluctuating inflow the direction of the resulting inlet velocity, and thus the mass flux into the domain is changing continuously. This change of the incoming mass flux demands for an immediate adaption of the mass flux at the outlet boundary in order to maintain global mass conservation and results in an immediate and unphysical jump of all velocities inside the computational domain. To overcome this problem, the inlet velocities would have to be continuously scaled in order to keep the incoming mass flux constant. A second drawback is the problem of timing. Using an O-mesh around the airfoil the inlet boundaries are located in an oval arc around the airfoil [see Figure 2 (right)], and thus each inlet cell varies in its x and y coordinates. In order to describe a uniform fluctuation in the velocity components of x and y (i.e. u and v) the inlet velocities have to be altered precisely in a certain time sequence.

The implementation of Method 2 does not contain those difficulties since the direction of the inlet velocity is always kept perpendicular to the y-axis of the CFD coordinate system and the incoming mass flux does not change. Figure 3 (right) shows the same flow situation as in Figure 3 (left) now using Method 2 instead of Method 1. Since the inlet velocity remains perpendicular to the y-axis of the CFD coordinate system the coordinate system has now to be rotated with $-\phi_{presc}$ towards the structural coordinate system. Due to the misaligned coordinate systems the aerodynamic forces have to be rotated with $-\phi_{presc}$ before they can be used inside the structural model. Vice versa, the structural motions have to be rotated with $+\phi_{presc}$ before they can be used inside the aerodynamic model.

A drawback of Method 2 is that rotating the airfoil instead of changing the direction of the inlet velocity in front of the airfoil is not identical since the additional rotation of the airfoil excerts additional work to the surounding flow. However, the added mass effect associated to this additional airfoil rotation is expected to be insignificant if its reduced

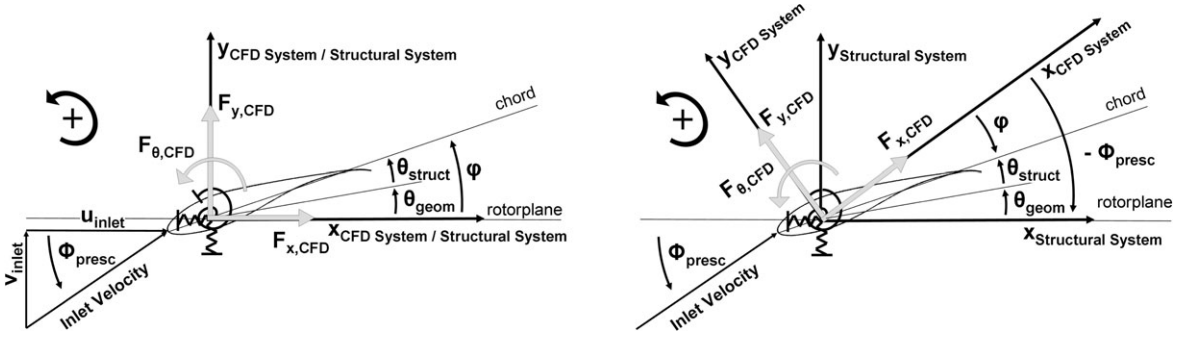

Figure 3. (left) Method 1: Flow angle ϕ_{presc} adjusted via u_{inlet} and v_{inlet}; (right) Method 2: Flow angle ϕ_{presc} adjusted via φ.

* The term ϕ_{presc} is used since this flow angle is prescribed by the known velocities V_a and V_{rot} and can be used as input for the simulations. The term stands in contrast to the general flow angle ϕ, which includes the initially unknown structural components $\dot{x}_{struct}$ and $\dot{y}_{struct}$ [see Figure 2 (left)].

† The inlet velocity is normalized with the free stream velocity $V_\infty = \sqrt{V_{rot}^2 + V_a^2}$ (see also Table II). In order to dimensionalize the obtained results correctly, it is thus important to note that V_∞ changes its magnitude at each time step.

frequency is $k \leq 0.05$ (see Leishmann[18]). To describe the fluctuating inflow used in the present work the airfoil rotates with a reduced frequency of less than $k = 0.015$. This is considerably below the limit given by Leishmann.

Due to the rather laborious changes necessary to implement Method 1 into the aerodynamic model it was decided to use Method 2 for the simulations of this work. In order to summarize and in order to compare the two discussed methods the several input parameters of the aerodynamic and the structural model are listed in Table II.

3.3. Verification of the aeroelastic model

Before implementing the control algorithms into the aeroelastic model the correct coupling of the structural with the aerodynamic model is verified by comparing the results with computations done with the aeroelastic model used in Buhl *et al*.[5] where the aerodynamic forces are computed with the potential flow solver developed by Gaunaa.[10] The observed test case simulates the aeroelastic response of the Risø B1–18 baseline airfoil (no flap attached) subjected to a sudden wind gust at $t = 1$ s, in which the axial wind velocity V_a increases from 10 m s^{-1} to 12 m s^{-1}. The rotational velocity is

Table II. Several input parameters of Method 1 and Method 2.

Method 1	Method 2
Input to the aerodynamic model:	Input to the aerodynamic model:
$v_{inlet} = \frac{V_{rot}}{V_\infty}$, $u_{inlet} = \frac{V_a}{V_\infty}$	$v_{inlet} = \frac{\sqrt{V_{rot}^2 + V_a^2}}{V_\infty} = 1$, $u_{\text{inlet}} = 0$
$\begin{bmatrix} r_x \\ r_y \end{bmatrix} = \begin{bmatrix} x_{struct} \\ y_{struct} \end{bmatrix}$	$\begin{bmatrix} r_x \\ r_y \end{bmatrix} = \mathbf{M} \begin{bmatrix} x_{struct} \\ y_{struct} \end{bmatrix}$
$\varphi = \theta_{geom} + \theta_{struct}$	$\varphi = \theta_{geom} + \theta_{struct} - \phi_{presc}$
Input to the structural model:	Input to the structural model:
$\begin{bmatrix} F_x \\ F_y \end{bmatrix} = \begin{bmatrix} F_{x,CFD} \\ F_{y,CFD} \end{bmatrix}$	$\begin{bmatrix} F_x \\ F_y \end{bmatrix} = \mathbf{M}^{-1} \begin{bmatrix} F_{x,CFD} \\ F_{y,CFD} \end{bmatrix}$
$F_\theta = F_{\theta,CFD}$	$F_\theta = F_{\theta,CFD}$
with $V_\infty = V_\infty = \sqrt{V_{rot}^2 + V_a^2}$ and $\mathbf{M} = \begin{bmatrix} \cos\phi_{presc} & \sin\phi_{presc} \\ -\sin\phi_{presc} & \cos\phi_{presc} \end{bmatrix}$	

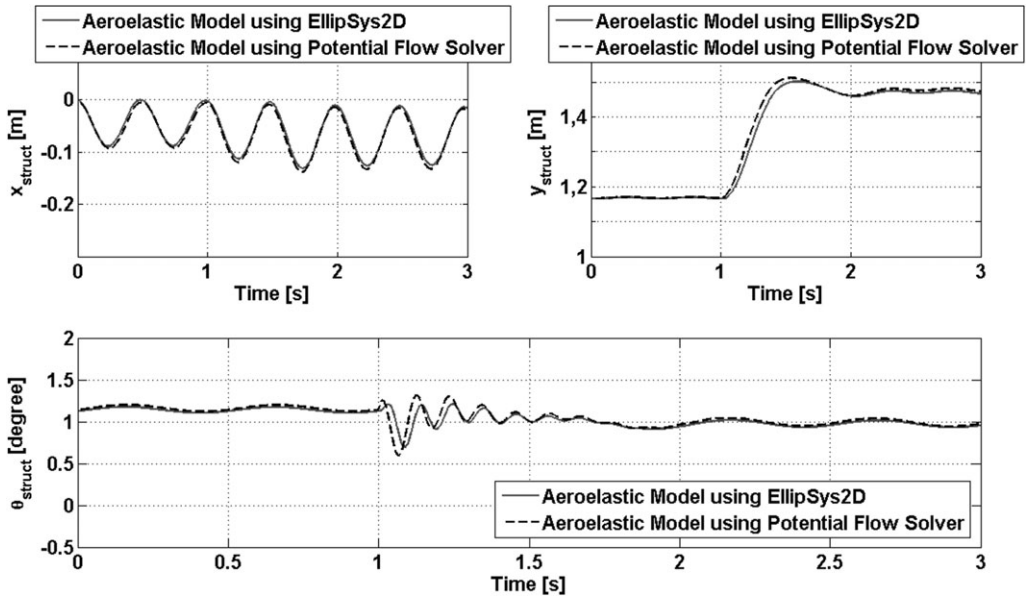

Figure 4. Structural response for a step change in V_a from 10 m s^{-1} to 12 m s^{-1} using EllipSys2D and a potential flow solver, respectively.

Wind Energ. 2011; **14**:449–462 © 2010 John Wiley & Sons, Ltd.
DOI: 10.1002/we

assumed to remain constant at $V_{rot} = 60$ m s^{-1}. In the CFD computations, the wind gust was simulated by pitching the blade with a velocity of $\dot{\phi}_{presc} = 40\ ^\circ$ s^{-1} in order to omit unrealistic transients. This corresponds to a ramp up time of 0.05 *s*. In the potential flow computations the wind gust is simulated as a sudden change in free stream velocity, which is felt immediately at all chord positions. The quantities of the structural model are the ones given in Table I.

The comparison for the computed structural responses is shown in Figure 4 and reveals a very good agreement between the two aeroelastic models. The oscillations before the step in wind speed, particularly recognizable in the nearly edgewise direction x_{struct}, are due to the initial conditions that obviously were not located at equillibrium. Since the aerodynamic damping in the edgewise direction is very low these initial oscilliations persist during the whole simulation run. The very good correspondance between the two models indicates a correct coupling between the 3 DOF structural model and EllipSys2D as well as a correct implementation of the further above explained method to simulate a fluctuating inflow.

3.4. The control

The two different flap controls investigated in this work are shown in Figure 5. While Control 1 uses the AOA at a certain distance d_1 in front of the airfoil, Control 2 uses the pressure difference measured at a certain chord position d_2 as input. The control algorithms for the two controls are very similar. For the two algorithms the measured quantities α_{meas} and Δp_{meas}, respectively, are compared to a certain reference value which is found by averaging the preceding measurements over a defined time window τ.* As long as α_{meas} or Δp_{meas} equals its reference value the flap remains at its middle position β_m. A deviation between the measured value and the reference value indicates a change of the aerodynamic loading and thus the flap is activated in order to counteract that effect. Looking at the control algorithms it can be seen that the sensitivity of the flap motion is adjusted via the control gains A_α and A_p, respectively. In the previous work of Buhl *et al.*[5] an additional factor of $(dC_l/d\alpha)/(dC_l/d\beta)$ was added to the pitot tube algorithm. This factor relates the change in AOA to a respective change in β in order to keep C_l constant. Using this factor should put the gain parameter A_α close to a non-dimensionalized value of 1. In the calculations of this work, the factor is set to a constant value of $(2\pi)/(-2rad^{-1})$ which is a rough estimate valid for an AOA measured in the undisturbed farfield of the flow. Both control algorithms are of the proportional-integrative (PI) controller type.[7]

Based on experiments the maximum actuation velocity of the piezoelectric flaps was estimated with $v_{\beta,up} = -520\ ^\circ$ s^{-1} for flapping up (towards negative flap angles) and $v_{\beta,down} = 130\ ^\circ$ s^{-1} for flapping down (towards positive flap angles). This corresponds to a maximum reduced flapping frequency of $k = 0.076$, and thus lies well below the reduced frequency of $k = 0.518$ for which the utilized grid and time step size was found to be suitable (see Heinz[8]). Information about the maximum acceleration of the flaps was not available, but in the simulations a maximum of $a_\beta = 10^5\ ^\circ$ s^{-2} is chosen. This value might still lie much above the real acceleration limit, but without this limitation the simulations with the pressure

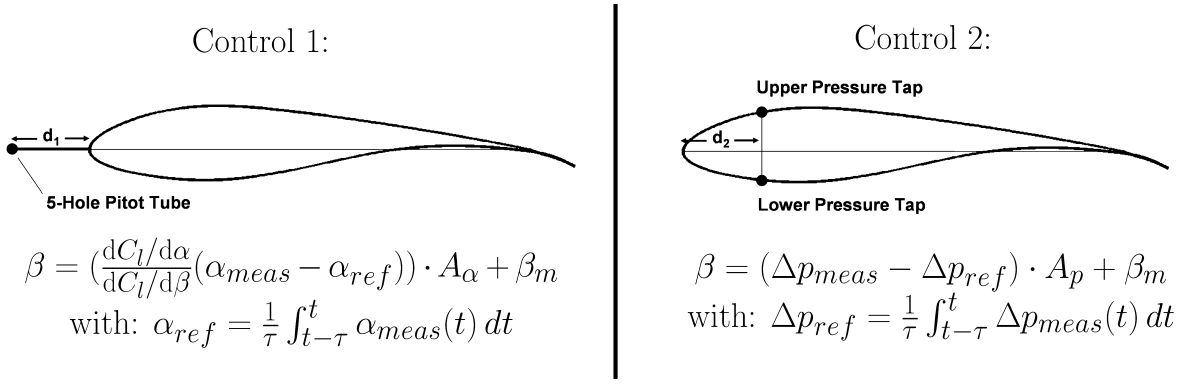

Figure 5. The two implemented controls.

* According to previous work the time window is chosen to be $\tau = 6$ s since this corresponds to a full blade rotation of a 10 MW turbine. Load variations which are slower than this 1P period are expected to be regulated by the pitch control. In order to limit the computational time the simulations shown in the results section are only 4 s in length. Thus, a constant value of the measured quantities determined at the initial wind speed is used to fill up the missing entries inside the averaging time window and to calculate the respective reference value.

difference control (Control 2) showed unrealistic fast oscillations in the flap motion and in the force signal. This was because the pressure distribution over the airfoil is immediately adapting to a change in the flap position. If Control 2 decides to flap up, a distinct pressure change is already measured at the very next time step of the simulation and might tell the flap to immediately flap down again. This tight coupling between flap motion and measured pressure difference leads to an oscillating flap motion which in reality is prevented by a certain acceleration limit of the flap and which thus asks for a respective acceleration limit in the simulations as well. The corresponding computations using Control 1 do not show this kind of behaviour since a change in the flap position needs much more time to affect the measured AOA in front of the airfoil.

3.5. Results

The 2D airfoil section equipped with the piezoelectric flap is now exposed to different wind situations namely a sudden wind step and a 4 s turbulent inflow signal. The efficiency of the control is evaluated by its potential to alleviate the fluctuations of the normal force F_y [see Figure 2 (right)] pointing into the nearly flapwise direction. The achievable load reduction $R_{Std(F_y)}$ is given in percentages and is found by comparing the computed standard deviations $Std(F_y)$ of the controlled and the uncontrolled case.

$$R_{Std(F_y)} = \frac{Std(F_y)_{uncontrolled} - Std(F_y)_{controlled}}{Std(F_y)_{uncontrolled}} \times 100\%$$

The optimal gains and thus the maximum load reductions for the several test cases are found by a gain sweep using an interval of $\Delta A_\alpha = 0.02$ and $\Delta A_p = 0.0005\ ^\circ\ \mathrm{Pa}^{-1}$, respectively, which is 2.5 times (Control 1) and 4 times (Control 2) smaller than the one used in Heinz.[8] The small gain intervalls are chosen to reassure that the found maximum load reductions indeed represent an optimum.

In contrast to Heinz[8] where the simulations were only carried out for a fixed Pitot tube length of $d_1 = 0.30c$ (with c being the chord length of the airfoil) and a fixed pressure tap position of $d_2 = 0.12c$, the optimum gain parameter and thus the highest load reduction potential is now determined for several Pitot tube lengths and several pressure tap positions in order to obtain information about the preferable measurement positions for the two controls. In a thorough parametric study Control 1 is investigated for several Pitot tube lengths starting with $d_1 = 0.05c$ as the shortest and ending with $d_1 = 1.50c$ as the longest Pitot tube. Respectively Control 2 is investigated for varying pressure tap positions between $d_2 = 0.03c$ and $d_2 = 0.45c$.

Wind step

The first step to investigate the load reduction potential is done by exposing the airfoil to a sudden wind change from 10 m s^{-1} to 10.5 m s^{-1}. In former studies such as Heinz,[8] it was seen that the optimal gains found during a wind step simulation also give a strong indication for the optimal gains of other (turbulent) inflow signals.

In Figure 6 (left) the calculated load reductions $R_{Std(F_y)}$ for Control 1 are plotted versus the respective gain parameters A_α. The maximum load reductions and its optimal gain parameters are listed in the first two columns of Table III. For all tested Pitot tube lengths the achieved load reductions are equally high with approximately $R_{Std(F_y)} = 95.5\%$. Even with very small Pitot tube lengths, where the AOA is measured close to the LE and where the flowfield is highly influenced by self-induction effects convincing results could be achieved. The closer the measurement point is located towards the LE the more pronounced is the change in the local AOA and the lower the gain parameters have to be chosen.

The results for the step change simulations using Control 2 are given in Figure 6 (right) and Table IV. For the pressure tap positions of $0.03c \le d_2 \le 0.15c$ the load reduction can be kept quite close to $R_{Std(F_y)} = 94\%$. However, the flat maxima at $d_2 = 0.12c$ and $d_2 = 0.15c$ promise an easier gain adjustment in real life and thus makes them the preferred measurement positions. The further the taps are located away from the leading edge, the higher the gains have to be chosen, since the change in the measured pressure difference Δp_{meas} is less pronounced, and relatively high gains are needed to obtain the desired flap deflection angles.

For chord positions of $d_2 \ge 0.20c$, the load reduction curves cease before they reach their absolute maxima. Simulations using higher gains could slightly increase the computed load reductions for those specific pressure tap positions, however, the results are not shown in the figure since an investigation of the corresponding force signals and flap angles showed very pronounced oscillations in those quantities. It seems unreasonable that despite those oscillations a higher load reduction is computed, but this is due to the definition of the standard deviation in the step change simulations where the deviation of the normal force F_y is calculated relative to its initial value at 10 m s^{-1}. While the non-oscillating force signals (using lower gains) remain slightly above the initial value, the oscillating force signals (using higher gains) are oscillating around the initial value and thus lower standard deviations and higher load reduc-

Wind Energ. 2011; **14**:449–462 © 2010 John Wiley & Sons, Ltd.
DOI: 10.1002/we

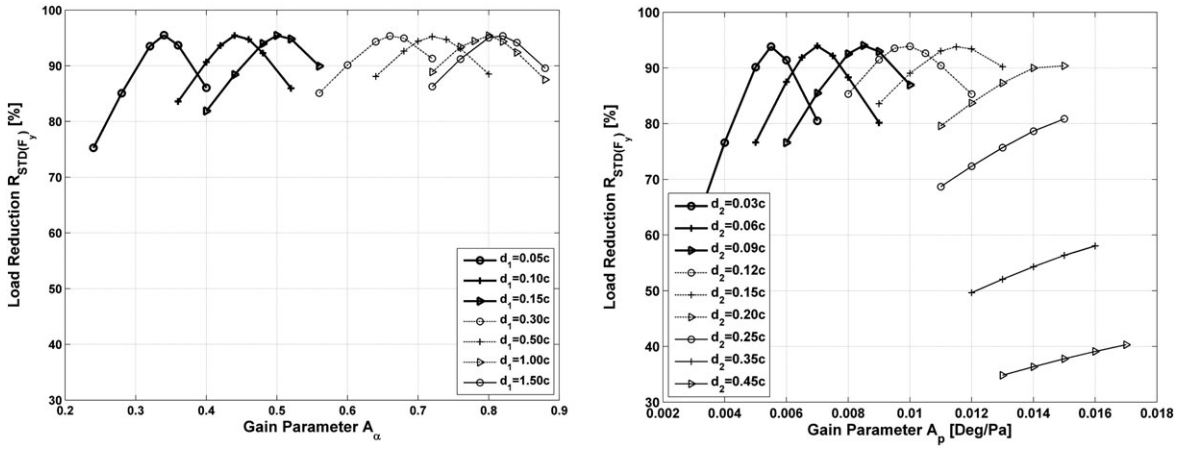

Figure 6. (left) Control 1: Load reduction $R_{Std(F_y)}$ for several Pitot tube lengths during a wind step from $V_a = 10$ m s^{-1} to $V_a = 10.5$ m s^{-1}; (right) Control 2: Load reduction $R_{Std(F_y)}$ for several chord positions during a wind step from $V_a = 10$ m s^{-1} to $V_a = 10.5$ m s^{-1}.

Table III. Control 1: Results for varying measurement positions.

	Wind Step		TI = 2.2% (t_{delay} = 0.00 s)		TI = 2.2% (t_{delay} = 0.02 s)	
d_1	$A_{\alpha,Opt}$	$R_{Std(F_y)}$ [%]	$A_{\alpha,Opt}$	$R_{Std(F_y)}$ [%]	$A_{\alpha,Opt}$	$R_{Std(F_y)}$ [%]
0.05c	0.34	95.50	0.34	76.69	0.32	70.44
0.10c	0.44	95.43	0.44	76.31	0.42	70.10
0.15c	0.50	95.45	0.50	75.95	0.48	69.81
0.30c	0.66	95.35	0.66	74.86	0.64	68.80
0.50c	0.72	95.25	0.72	73.68	0.70	67.62
1.00c	0.80	95.43	0.78	71.35	0.76	65.05
1.50c	0.82	95.57	0.80	70.08	0.78	63.33

Table IV. Control 2: Results for varying measurement positions.

	Wind Step		TI = 2.2% (t_{delay} = 0.00 s)		TI = 2.2% (t_{delay} = 0.02 s)	
d_2	$A_{p,Opt}$ [°/Pa]	$R_{Std(F_y)}$ [%]	$A_{p,Opt}$ [°/Pa]	$R_{Std(F_y)}$ [%]	$A_{p,Opt}$ [°/Pa]	$R_{Std(F_y)}$ [%]
0.03c	0.0055	93.85	0.0055	74.45	0.0055	68.88
0.06c	0.0070	93.95	0.0070	75.27	0.0070	69.66
0.09c	0.0085	94.04	0.0085	76.22	0.0085	70.69
0.12c	0.0100	93.89	0.0100	76.94	0.0095	71.52
0.15c	0.0115	93.79	0.0115	77.69	0.0115	72.51
0.20c	0.0130	87.30	0.0140	77.36	0.0150	74.21
0.25c	0.0130	75.70	0.0160	74.45	0.0190	74.39
0.35c	0.0140	54.32	0.0210	58.79	0.0200	55.76
0.45c	0.0150	37.79	0.0200	34.63	0.0160	31.00

tions are computed. However, these oscillations are not desirable and the gain values are kept at lower values where no flap and force oscillations occur. It should be mentioned here that the described oscillations had relatively low frequencies and were clearly related to the chosen gains leading to an unstable control. They were not related to the chosen time step size ($\Delta t^* = 0.01$).

Turbulent inflow

The same load reduction investigations are now carried out for a 4 s time series of turbulent inflow with a turbulence intensity of $TI = 2.2\%$ and a mean wind speed of $V_{mean} = 10.2$ m s^{-1} (see Figure 7). The turbulence intensity is chosen in

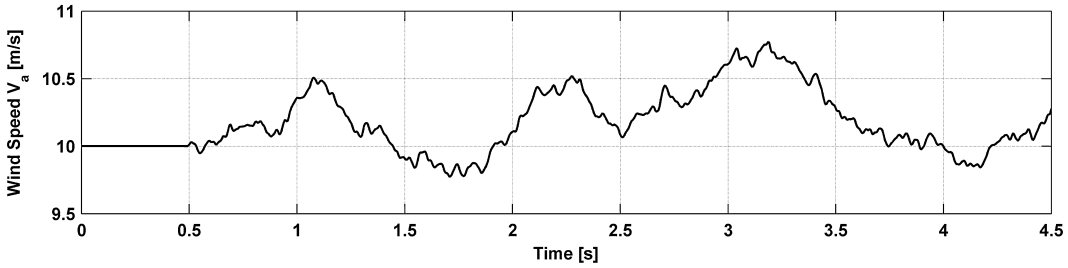

Figure 7. 4 s time series of the turbulent inflow signal with TI = 2.2%.

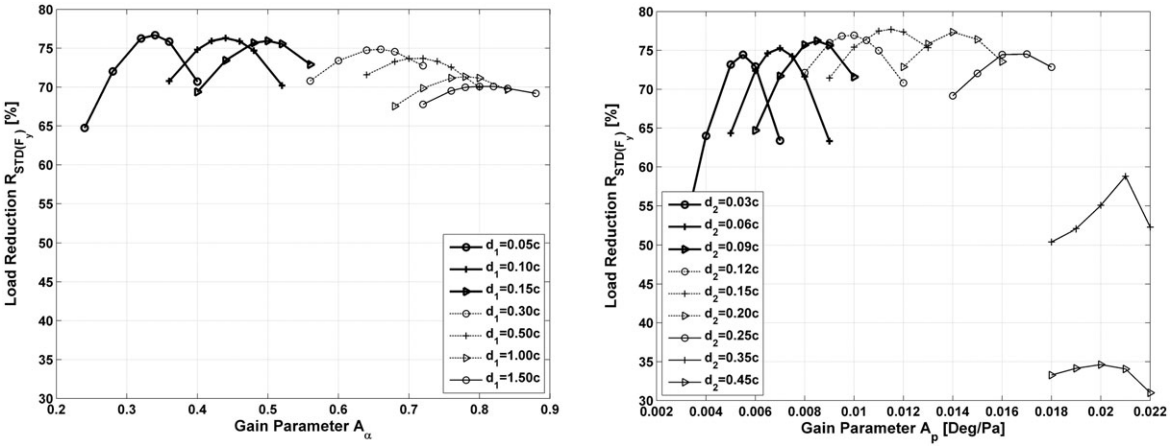

Figure 8. (left) Control 1: Load reduction $R_{Std(F_y)}$ for several Pitot tube lengths during a 4 s turbulent inflow with TI = 2.2% and V_{mean} = 10.2 m s^{-1}; (right) Control 2: Load reduction $R_{Std(F_y)}$ for several chord positions during a 4 s turbulent inflow with TI = 2.2% and V_{mean} = 10.2 m s^{-1}.

accordance to the maximum flap angles of the piezoelectric flaps since the changes in lift force due to $TI = 2.2\%$ can be counteracted by the flap without reaching its deflection limits. The given wind speed signal results in angles of attack between 4.2° and 5.3° (not taking the influence of θ_{struct} into account) and the simulations are thus carried out under attached flow conditions. It is assumed that the pitch system takes care of the larger turbulence scales and provides a well attached flow with rather small variations in AOA at the outer part of the blade, where trailing edge flaps should preferably be installed.

In Heinz[8] the piezoelectric flaps were also tested for higher turbulence intensities of up to $TI = 7.7\%$ where the reduction of flapwise oscillations was still 54%. However, it was decided to not include those cases into the present parameter studies since they might be better treated with models of future flap mechanisms with higher flap ranges. Generally the utilized aero-servo-elastic simulation model is well suited to also investigate higher angles of attack and higher flap angle ranges.

In Figure 8 (left), the results for Control 1 are shown and the exact values are listed in the third and forth column of Table III. As expected, the optimum gain parameters are nearly identical with the ones already determined in the step change simulations. The achievable load reduction gradually increases with decreasing Pitot tube length and has a maximum of $R_{Std(F_y)} = 76.69\%$ for $d_1 = 0.05c$. The decrease of efficiency with an increasing length of the Pitot tube can be explained with the increasing motion of the measurement point for a certain structural rotation θ_{struct} of the blade section. The more the tip of the Pitot tube is moving, the higher are the additional velocity components, which then overlay and disturb the actual AOA measurements. The load reduction curves of the longer Pitot tubes have a smaller curvature, which indicates that the gain adjustment should be easier.

The investigations for Control 2 [Figure 8 (right)] reveal the best load reduction potential at a chord position of $d_2 = 0.15c$ where a load reduction of $R_{Std(F_y)} = 77.69\%$ can be achieved, however, all simulations with $d_2 \leq 0.25c$ give quite good results. The optimum measurement position at $d_2 = 0.15c$ is quite close to the proposed position

Wind Energ. 2011; **14**:449–462 © 2010 John Wiley & Sons, Ltd.
DOI: 10.1002/we

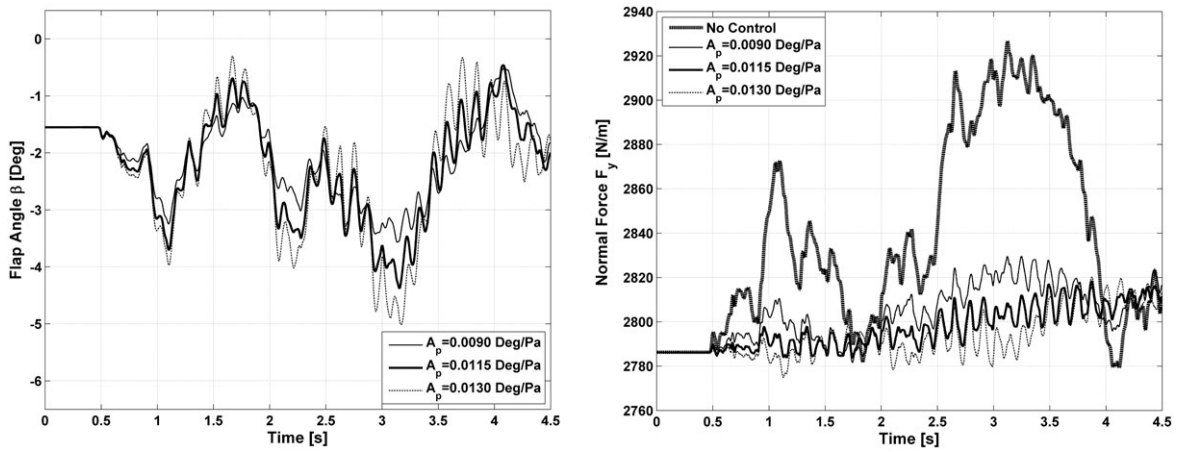

Figure 9. Flap angle β (left) and Normal force F_y (right) during a 4 s turbulent inflow with V_{mean} = 10.2 m s^{-1} and TI = 2.2% (Control 2, $d_2 = 0.15c$).

of Gaunaa[9] where the optimum pressure tap position, using thin airfoil potential flow theory, was determined with $d_2 = 0.125c$.*

Up to a chord position of $d_2 = 0.15c$, the optimum gains correspond exactly to those found in the step change simulations. As already observed there, the control seems to be more sensitive towards gain variations when the pressure taps are located close to the leading edge. Additionally the load reduction potential drops slightly for those pressure taps. The results for $d_2 \geq 0.35c$ are decisively worse.

In Figure 9, the simulated flap motions and the corresponding force signals at a pressure tap position of $d_2 = 0.15c$ are shown for three selected gain parameters. In Figure 9 (left), it can be seen how the flap moves away from its initial middle position at $\beta = -1.55°$ in order to level out the variations in the lift force. For a gain parameter of $A_p = 0.0115$ ° Pa^{-1}, the variation in the lift force is minimized. For higher gain parameters such as $A_p = 0.0130$ ° Pa^{-1}, the flap motion show higher amplitudes and the control is close to instability.

Time delay investigations

In a real control, there is always a certain time needed to process the measured signal of the pressure taps or the Pitot tube and to actuate the piezoelectric flap. In previous work such as Buhl *et al.*[5] and Heinz,[8] this time delay was found to be very decisive for the achievable load reduction and is thus also investigated in the present work.

The simulations for the turbulent inflow of the previous section are now carried out by assuming a time delay of $t_{delay} = 0.02$ s. In former investigations the losses for such a time lag were still moderate whereas longer time delays, at least for the pressure tap control, could already lead to an unstable response (see Heinz[8]). The results are plotted in Figure 10, the optimum values are given in Table III and Table IV, respectively. Comparing the computed load reductions of Control 1 with the results for $t_{delay} = 0.00$ s shows a nearly constant loss in load reduction of approximately $\Delta R_{Std(F_y)} = 6\%$ for all tested Pitot tube lengths. The optimum gain parameters are slightly lower than the respective parameters determined in the simulations without time delay.

For Control 2 and $d_2 \leq 0.15c$ the loss in load reduction is also close to $\Delta R_{Std(F_y)} = 6\%$ and the gain parameters are nearly identical to the ones for $t_{delay} = 0.00$ s. For $d_2 = 0.20c$ the loss is only $\Delta R_{Std(F_y)} = 3\%$ and for $d_2 = 0.25c$ there is even no difference to the result without time delay. The good performance at $d_2 = 0.25c$ is connected to the fact that the gain parameter can be increased without getting an unstable control. For the simulations with $d_2 > 0.25c$, the performances decrease rapidly.

A last investigation is carried out for the fixed measurement positions at $d_1 = 0.30c$ (Control 1) and $d_2 = 0.15c$ (Control 2) with gradually increasing time delays of $t_{delay} = 0.01$ s, 0.02 s, 0.04 s, 0.07 s and 0.10 s.

The results are shown in Figure 11 and in Table V. It seems that until a time delay of $t_{delay} = 0.04$ s the loss in load reduction for both controls is nearly linearly correlated with the introduced time delay. The degradation rate is approximately 0.30% ms^{-1}. In contrast to previous time delay investigations Control 2 is also stable for $t_{delay} > 0.04$ s since the gain parameters are readjusted for each simulation. For both controls the load reduction for $t_{delay} = 0.10$ s are higher than for $t_{delay} = 0.07$ s, since the gain parameters could be increased before reaching an unstable response.

* Gaunaa pointed out that the pressure difference at this position is not influenced by the time rate of change of AOA and is thus better correlated to the actual AOA and lift force. This makes it the preferable measurement position for the control input since the control is judged by its ability to reduce the variations in lift.

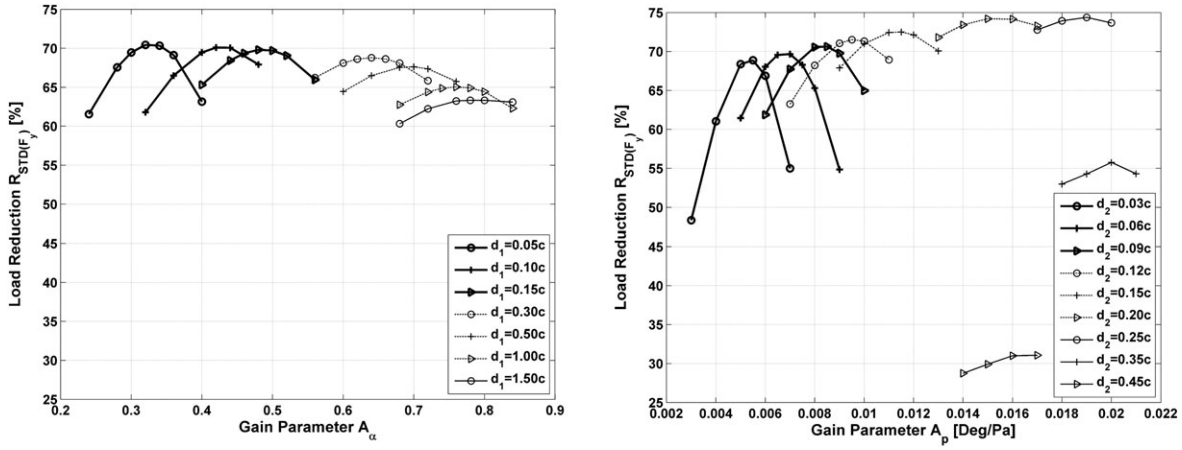

Figure 10. (left) Control 1: Load reduction $R_{Std(F_y)}$ for several Pitot tube lengths during a 4 s turbulent inflow with V_{mean} = 10.2 m s^{-1}, TI = 2.2% and t_{delay} = 0.02 s; (right) Control 2: Load reduction $R_{Std(F_y)}$ for several chord positions during a 4 s turbulent inflow with V_{mean} = 10.2 m s^{-1}, TI = 2.2% and t_{delay} = 0.02 s.

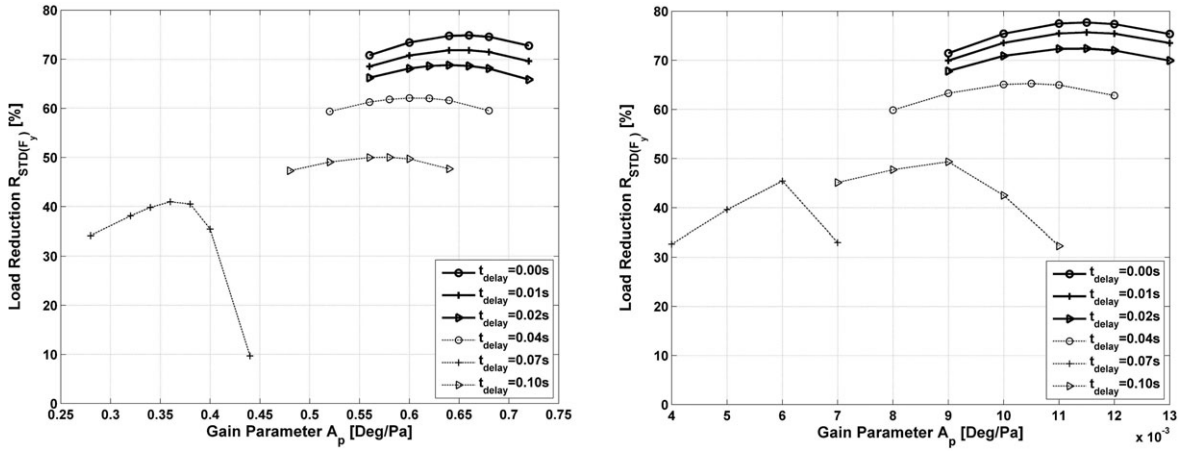

Figure 11. Load reduction $R_{Std(F_y)}$ for several time delays t_{delay} during a 4 s turbulent inflow with V_{mean} = 10.2 m s^{-1}, TI = 2.2% for: (left) Control 1 and d_1 = 0.30c; (right) Control 2 and d_2 = 0.15c.

Table V. Time Delay Investigation at fixed measurement positions.

	Control 1 (at d_1 = 0.30c)		Control 2 (at d_2 = 0.15c)	
t_{delay} [s]	$A_{\alpha,Opt}$	$R_{Std(F_y)}$ [%]	$A_{p,Opt}$ [°/Pa]	$R_{Std(F_y)}$ [%]
0.00	0.66	74.87	0.0115	77.69
0.01	0.66	71.82	0.0115	75.67
0.02	0.64	68.80	0.0115	72.38
0.04	0.60	62.09	0.0105	65.27
0.07	0.36	40.97	0.0060	45.41
0.10	0.58	50.02	0.0090	49.33

4. CONCLUSION

A 2D aero-servo-elastic model using the 2D CFD code EllipSys2D for the aerodynamic modelling was utilized to compare the load reduction potential of two different flap controls with different input signals. While Control 1 measures the AOA with a Pitot tube attached in front of the leading edge, Control 2 measures the pressure difference between the suction and pressure side at a certain chord position.

Wind Energ. 2011; **14**:449–462 © 2010 John Wiley & Sons, Ltd.
DOI: 10.1002/we

The investigations were carried out under attached flow conditions and revealed a very good load reduction potential for both tested controls. For a 4 s simulation and a turbulent inflow with TI = 2.2% Control 1 shows a maximum load reduction of $R_{Std(F_y)} = 76.7\%$. This result was achieved for a Pitot tube length of 0.05 times the chord length c, which was thereby also the shortest Pitot tube in the studies. Control 2 shows its highest load reduction of $R_{Std(F_y)} = 77.7\%$ at a chord position of $0.15c$, which is quite close to the proposed position of Gaunaa[9] where the optimum pressure tap position, using thin airfoil potential flow theory, was determined with $d_2 = 0.125c$.

For a time delay of $t_{delay} = 0.02$ s the simulations for Control 1 show a loss in load reduction of approximately $\Delta R_{Std(F_y)} = 6\%$. This result is independent from the Pitot tube length. For pressure tap positions smaller and equal to $0.15c$ Control 2 has a similar loss in load reduction. For the chord positions of $0.20c$ and $0.25c$ the loss decreases and nearly disappears, respectively. Simulations for different time delays with a fixed Pitot tube length of $0.30c$ and a fixed pressure tap position of $0.15c$ revealed a nearly linear loss in load reduction of 0.30% ms^{-1} (for time delays $t_{delay} \leq 0.04$ s).

The gain parameters determined during a basic step change in wind speed are also valid for other (turbulent) inflow signals. With increasing time delay the gain parameters slightly decrease. An exception was observed for Control 2 at the measurement positions of $0.20c$ and $0.25c$ where the gain parameters could be further increased without reaching an unstable control.

ACKNOWLEDGEMENT

This work is part of the Danish ATEF—project financed by the Danish High Technology Foundation (Højteknologifonden).

NOMENCLATURE

c	Chord length [m]
c_x, c_x, c_θ	Damping coefficients [Ns/m], [Ns/m], [Ns/rad]
d_1, d_2	Measurement positions of Control 1, Control 2 [m]
k	Reduced frequency [–], $k = \omega c/(2U)$
k_x, k_y, k_θ	Spring stiffnesses [N/m], [N/m], [N/rad]
x_{struct}, y_{struct}	Structural deflections of the blade [m]
k_x, k_y, k_θ	Spring stiffnesses [N/m], [N/m], [N/rad]
A_α, A_p	Gain parameters of Control 1, Control 2 [–], [°/*Pa*]
C_l	Lift coefficient [–]
F_x, F_y, F_θ	Aerodynamic forces in structural CS [N], [N], [Nm]
$F_{x,CFD}$, $F_{y,CFD}$, $F_{\theta,CFD}$	Aerodynamic forces in CFD CS [N], [N], [Nm]
$R_{Std(F_y)}$	Load reduction in F_y [%]
V_a	Axial wind speed [m/s]
V_{rot}	Rotational velocity of blade [m/s]
α	Angle of attack [°]
α_{meas}	Measured angle of attack [°]
β	Flap deflection angle [°]
θ_{geom}	Pitch angle of blade [°]
θ_{presc}	Prescribed flowangle (excl. struct. motion) [°], $\theta_{presc} = \arctan(V_a/V_{rot})$
θ_{struct}	Structural deflection of the blade around RC [°]
φ	Rotational angle of moving mesh [°]
Δp_{meas}	Measured pressure difference [*Pa*]
Δt^*	Non-dimensionalized time step [–]
AOA	Angle of attack
ATEF	Adaptive trailing edge flaps
CG	Centre of gravity
Control 1	Pitot tube control
Control 2	Pressure difference control
CS	Coordinate system
DOF	Degree of freedom
LE	Leading edge

RC	Rotational centre
Std	Standard deviation
TE	Trailing edge

REFERENCES

1. Larsen T, Madsen H, Thomsen K. Active Load Reduction using Individual Pitch, Based on Local Blade Flow Measurements. *Wind Energy Journal* 2005; **8**: 67–80.
2. Barlas TK, van Kuik GAM. State of the Art and Prospectives of Smart Rotor Control for Wind Turbines. *Journal of Physics: Conference Series* 2007; **75**: 012080.
3. R. Chow and C. P. van Dam. Computational investigations of small deploying tabs and aerodynamic load control. *Journal of Physics: Conference Series* 2007; **75**: 012027–1–10.
4. Nakafuji DTY, van Dam C, Smith R, Collins S. Active load control for airfoils using microtabs. *Journal of Solar Energy Engineering* 2001; Vol. 123. 282–289.
5. Buhl T, Gaunaa M, Bak C. Potential load reduction using airfoils with variable trailing edge geometry. *Journal of Solar Energy Engineering* 2005; **127**: 503–516.
6. Bak C, Gaunaa M, Andersen PB, Buhl T, Hansen P, Clemmensen K, Moeller R. Wind Tunnel Test on Wind Turbine Airfoil with Adaptive Trailing Edge Geometry. *45th AIAA/ASME* 2007; **18**: 12314–12325.
7. Andersen PB. Load alleviation on wind turbine blades using variable airfoil geometry (2D and 3D study). Technical University of Denmark, 2005.
8. Heinz J. Investigation of piezoelectric flaps for load alleviation Using CFD. Risø-R-1702(EN), Risø DTU National Laboratory, 2009.
9. Gaunaa M, Andersen PB. Load reduction using pressure difference on airfoil for control of trailing edge flaps. EWEC 2009, 2009.
10. Gaunaa M. Unsteady 2D potential-flow forces on a thin variable geometry airfoil undergoing arbitrary motion. Risø-R-1478,Denmark, 2004.
11. Michelsen JA. Basis3D—a Platform for Development of Multiblock PDE Solvers. Tech. Report AFM 92-05, Technical University of Denmark, 1992.
12. Michelsen JA. Block structured multigrid solution of 2D and 3D elliptic PDEs. Tech. Report AFM 94-06, Technical University of Denmark, 1994.
13. Sørensen NN. General purpose flow solver applied to flow over hills. Risø National Laboratory, 1995.
14. Ferziger JH, Peric M. *Numerische Strömungsmechanik*. Springer Verlag: Berlin, Heidelberg, 2008.
15. Menter FR. Two-equation eddy-viscosity turbulence model for engineering applications. *AIAA Journal* 1994; **32**: 269–289.
16. Menter FR. Performance of popular turbulence models for attached and separated adverse pressure gradient flows. *AIAA Journal* 1992; **30**: 2066–2072.
17. Sørensen NN. HypGrid2D a 2-D Mesh Generator. Risø-R-1035(EN), Risø National Laboratory, 1998.
18. Leishman JG. *Principles of Helicopter Aerodynamics*. Cambridge University Press: New York, 2006.

Wind Energ. 2011; **14**:449–462 © 2010 John Wiley & Sons, Ltd.
DOI: 10.1002/we